ORIGINAL RESEARCH

Sulfonated poly(fluorenyl ether ketone)/Sulfonated α-zirconium phosphate Nanocomposite membranes for proton exchange membrane fuel cells

Hang Hu[1] · Fuchuan Ding[2,3,4] · Hao Ding[2,3] · Jingjing Liu[2,3] · Min Xiao[5] · Yuezhong Meng[5] · Luyi Sun[2,3]

Abstract

Sulfonated poly(aryl ether) (SPAE) membranes have attracted significant attention as polymer electrolyte membranes due to their superior mechanical properties and low cost. However, the poor chemical stability and methanol barrier property of SPAE membranes limit the fuel cell performance. It is necessary to improve the proton conductivity, methanol barrier property, and stability of SPAE for high-performance fuel cells. Herein, a novel proton conductive filler, sulfonated α-zirconium phosphate (ZrP-SO$_3$H), was synthesized and introduced to sulfonated poly(fluorenyl ether ketone) (SPFEK) to fabricate advanced nanocomposite membranes. The oxidative stability, methanol permeability, water uptake, and proton conductivity of the as-prepared nanocomposite membranes were characterized. The nanocomposite membranes exhibited comparable performance as Nafion® 117 membrane in H$_2$/O$_2$ fuel cell and higher performance than Nafion® 117 in direct methanol fuel cell. These results suggest that ZrP-SO$_3$H-doped SPFEK membrane is a promising candidate as a proton exchange membrane in high-performance fuel cells.

Keywords Proton exchange membrane · α-zirconium phosphate · Fuel cell · Methanol permeability · Sulfonated α-zirconium phosphate

✉ Yuezhong Meng
  mengyzh@mail.sysu.edu.cn

✉ Luyi Sun
  luyi.sun@uconn.edu

1   Key Laboratory for Biobased Materials and Energy of Ministry of Education, College of Materials and Energy, South China Agricultural University, Guangzhou 510642, Guangdong, China

2   Polymer Program, Institute of Materials Science, University of Connecticut, Storrs, CT 06269, USA

3   Department of Chemical and Biomolecular Engineering, University of Connecticut, Storrs, CT 06269, USA

4   College of Chemistry and Materials Science & Fujian Key Laboratory of Polymer Science, Fujian Normal University, Fuzhou 350007, Fujian, China

5   Key Low Carbon Chemistry & Energy Conservation of Guangdong Province, State Key Laboratory Optoelectronic Materials & Technologies, School of Materials Science and Engineering, Sun Yat-Sen University, Guangzhou 510275, Guangdong, China

1 Introduction

Fuel cell (FC) technology has become increasingly important in recent years as fuel cells provide the highest energy density with low pollution, leading us to a power source revolution [1, 2]. One of the focuses in the development of FC technology is the proton exchange membrane (PEM). In the field of proton exchange membrane fuel cells (PEMFCs), PEM acts as a separator for the reactants, as well as a catalyst support, and at the same time provides ionic pathways for proton transport [3–5]. Up to now, it is generally accepted that poly(perfluoroalkyl sulfonic acid) (Nafion®) is the current benchmark material for the PEM due to its outstanding overall properties [6–8]. However, it has some disadvantages, including high cost, high methanol permeability, and poor performance at temperatures above 80 °C, which calls for the development of new membrane materials [9, 10].

In this respect, various sulfonated poly(aryl ether)s (SPAEs) have been extensively explored as PEM candidates with low cost and high performance [11–14]. Nevertheless, most of these SPAEs cannot meet the requirements in durability and proton conductivity. Because of the less pronounced hydrophilic/

hydrophobic phase separation in SPAEs compared with that in Nafion®, the proton transport channels in these SPAE membranes are narrower and more distorted. As a result, the proton transport efficiency is lower based on the same ion exchange capacity (IEC) [15]. Sulfonated poly(fluorene ether ketone) (SPFEK), which has been reported as a PEM in FCs, possesses acceptable proton conductivity and stability, but still not comparable with Nafion® [16]. In order to achieve considerable proton conductivity, a high sulfonation degree is required, but unfortunately, it sacrifices durability and dimensional stability. Until now, lots of methods have been introduced to improve the overall performance of these materials, such as hybridization [17, 18], acid-base blending [19, 20], surface coating [21, 22], and cross-linking [23, 24]. One of the most adopted approaches is hybridization, developing composite membranes composed of sulfonated polymeric ionomers and hygroscopic inorganic fillers. SiO_2 [25], ZrO_2 [26, 27], clays [28], α-zirconium phosphate (α-ZrP) [29, 30], and graphene oxide [31] have been incorporated into neat membranes by either directly dispersing the inorganic fillers in the PEM solution and followed by solution casting or impregnating the inorganic fillers into the porous structure of membranes. Most nanofillers typically improve the mechanical properties of the membranes owing to the nano-reinforcing effect but lower the proton conductivity because such nanofillers are not proton conductive [29, 31–33]. Although some proton conductive fillers, such as α-ZrP, have been examined, the composite membrane performance is still far from satisfactory, primarily because of the much lower proton conductivity of the inorganic fillers compared with Nafion® and other PEMs.

In this work, we synthesized sulfonic acid functionalized ZrP ($ZrP-SO_3H$) single-layer nanosheets as robust solid acid fillers for PEMs. The incorporation of such solid acid filler not only improves thermal stability and barrier properties but also offers additional protogenic groups for acid-water clusters, which is beneficial for proton transport [34, 35]. The morphology, water uptake, oxidative property, thermal stability, proton conductivity, and single-cell performance of the composite membranes were thoroughly investigated.

2 Experimental

2.1 Materials

Zirconyl chloride octahydrate ($ZrOCl_2 \cdot 8H_2O$, 98%, Aldrich), tetra-n-butylammonium hydroxide (TBA, 1.0 M in methanol, Aldrich), (3-mercaptopropyl)trimethoxysilane (MPTMS, 95%, Aldrich), and phosphoric acid (85%, Aldrich) were used as received without further purification. 4,4′-Difluorobenzophenone (DFBP, Aldrich) and 9,9′-bis(4-Hydroxypheyl) fluorene (BHF, Aldrich) were recrystallized from toluene and ethanol, respectively. Reagent-grade sulfuric acid (50%), ethanol, hydrochloric

acid, potassium hydroxide, sodium chloride, and hydrogen peroxide (30 wt.%) were obtained from commercial sources and used as received. Dimethylacetamide (DMAc) was dried over 4A molecule sieves, and toluene was dried over sodium wire prior to use. Anhydrous potassium carbonate was dried in a vacuum oven at 150 °C for 10 h.

2.2 Preparation of ZrP-SO₃H Nanosheets

ZrP micro-crystals were synthesized via the one-step hydrothermal method as reported [36–42]. Briefly, 6.0 g of $ZrOCl_2 \cdot 8H_2O$ was mixed with 60.0 mL 6.0 M H_3PO_4 in a sealed Teflon-lined pressure vessel. The mixture was reacted at 200 °C for 24 h, and the lateral dimensions of the synthesized ZrP micro-crystals are $600 \sim 800$ nm [38, 39].

ZrP micro-crystals were exfoliated into individual single-layer nanosheets using TBA as the exfoliation agent [43–48]. A sample of 0.50 g of ZrP was dispersed in 20.0 mL of deionized water with the assistance of ultrasonication (1 h). In an ice bath, 16.7 mL of 0.1 M TBA was added to the mixture, followed by 1 h of magnetic stirring and then another 1 h of ultrasonication. After that, a transparent liquid was obtained as exfoliated ZrP. In order to recover the acidic –OH groups on the ZrP nanosheet surface, a pre-determined amount of HCl solution (50% in excess) was introduced. An exfoliated ZrP gel was then collected by centrifugation and was sequentially rinsed three times with water, acetone, and toluene. A toluene dispersion containing ZrP nanosheets was obtained by treating the final product in toluene via ultrasonication.

As depicted in Fig. 1, the synthesized ZrP nanosheets were functionalized via a grafting reaction [49, 50]. In a 500-mL flask equipped with a condenser, 300 mL of ZrP dispersion (in toluene, containing 0.9 g of ZrP) was mixed with 14.73 g (75 mmol) of MPTMS. The dispersion was refluxed and stirred for 24 h in a N_2 atmosphere. The solid product was obtained by centrifuge, rinsed three times with toluene, filtered, and vacuum dried. The MPTMS functionalized ZrP nanosheets are denoted as ZrP-SH. The thiol groups of ZrP-SH were then further oxidized by H_2O_2 to form sulfuric acid groups according to the following procedures: 0.42 g ZrP-SH and 12.0-mL methanol were added to a flask, and 5.5 mL of H_2O_2 was introduced dropwise under a N_2 atmosphere. The reaction was kept at room temperature for 24 h. The mixture was filtered, and the obtained solid was rinsed with water and ethanol. After being vacuum dried and ground, $ZrP-SO_3H$ nanosheets were obtained. The procedures to synthesize $ZrP-SO_3H$ are illustrated in Fig. 1a.

2.3 Preparation of SPFEK/ZrP-SO₃H composite membranes

Disodium salt of 3,3′-disulfonated-4,4′-difluorobenzophenone (SDFBP) was synthesized according to the procedures
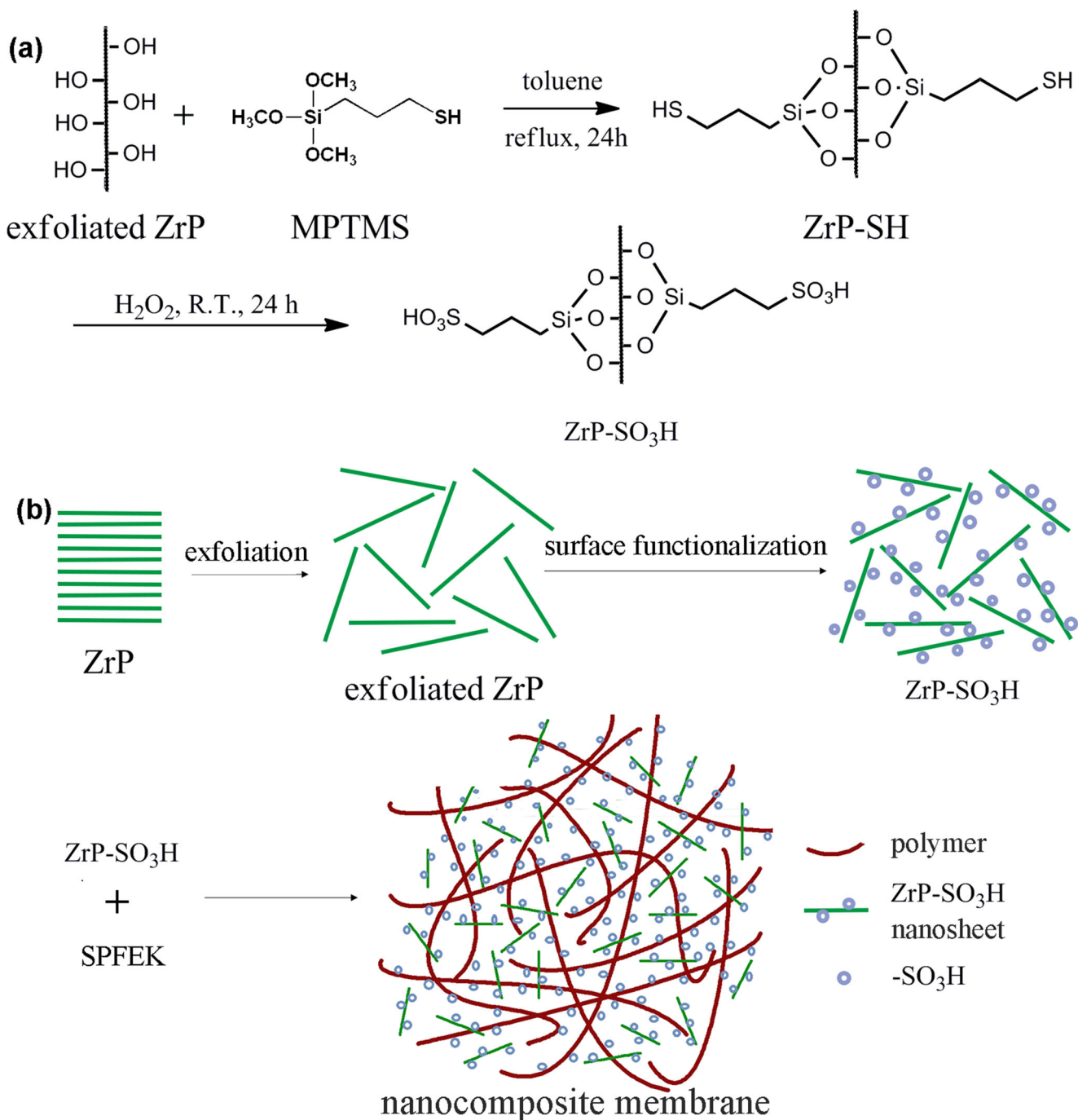
Fig. 1 a Procedures to functionalize ZrP to prepare ZrP-SO$_3$H nanosheets. b Procedures to prepare SPFEK/ZrP-SO$_3$H nanocomposite membrane

described by Wang et al [51]. SPFEK polymer matrix was prepared following the procedures described earlier [16]. The SPFEK/ZrP-SO$_3$H-x (x refers to the weight percentage of ZrP-SO$_3$H, x = 2, 4) composite membranes were prepared by casting from the SPFEK/ZrP-SO$_3$H DMAc uniform dispersion, which was achieved by ultrasonication. The dispersion was spread on a glass plate, left in a dust-free oven at 75 °C for 24 h, and then at 100 °C under vacuum for another 12 h. The synthesized sodium-form membranes were protonated after soaked in 0.50 M H$_2$SO$_4$ aqueous solution at 80 °C

for 24 h. Excessive acid was removed by washing the membrane in deionized water at 80 °C for 24 h. The acidified membranes were dried in a vacuum oven at 90 °C for 12 h. The thickness of all membranes was controlled in the range of 80–100 μm.

2.4 Membrane characterization

Fourier-transform infrared (FT-IR) spectra were recorded on a PerkinElmer Spectrum 100 Fourier transform

spectrophotometer to confirm the chemical structure of the components in the composite membranes. The membrane micro-morphology was examined using a scanning electron microscopy (SEM, JSM-5600LV system of JEOL) equipped with an energy dispersive X-ray detector (EDX). The accelerating voltage was 15 kV. The cross-sections were obtained via cryo-fracturing in liquid nitrogen. The thermal stability of the composite membranes was analyzed using a PerkinElmer Pyris Diamond thermogravimetric analyzer (TGA) in N_2 atmosphere. The temperature was increased from 50 to 150 °C and held for 20 min to eliminate the absorbed water and cooled to 50 °C and then elevated to 500 °C, all at a heating rate of 10 °C min^{-1}.

2.5 Water uptake

The dry membranes were weighed and immersed in deionized water at 80 °C for 24 h. The water uptake is calculated according to the following equation:

$$W\ (\%) = \frac{(W_w - W_d)}{W_d} \times 100\% \tag{1}$$

where W_d and W_w are the weight of the membranes before and after water absorption, respectively.

2.6 Ion exchange capacity (IEC)

IEC was measured by titration [52]. The membranes in acid form were immersed in a NaCl solution (2.0 M) for 10 h to replace the protons of sulfonic acid groups with sodium ions. The solutions were titrated using a NaOH solution (0.025 M), with phenolphthalein as an indicator. The moles of the proton denote the moles of the sulfonic groups, and the IEC is calculated from the titration data using the following equation:

$$IEC = \frac{\Delta V_{NaOH} C_{NaOH}}{W_s}\ \left(mol\ g^{-1}\right) \tag{2}$$

where W_s is the dry membrane weight, ΔV_{NaOH} is the consumed volume of the NaOH solution, and C_{NaOH} is the concentration of the NaOH solution.

2.7 Oxidative stability

A piece of the membrane (1×4 cm^2) was immersed in Fenton's reagent (3% H_2O_2 + 2 ppm $FeSO_4$) in a shaking bath (ZHICHENG ZHWY-110X water bath shaker) at 80 °C and kept for 1 h. The weight and IEC of the membranes before and after being treated in Fenton's reagent were tested to evaluate the oxidative stability.

2.8 Proton conductivity

The membranes were kept in deionized water overnight prior to each test. The proton conductivity (σ) was measured on a Solartron 1255 B frequency response analyzer coupled with a Solartron 1287 electrochemical interface. The impedance spectrum of a cell with the given membrane sample sandwiched between two gold electrodes was tested. After curve-fitting from the spectrum, the conductivity was calculated using the following equation:

$$\sigma = \frac{d}{RS} \tag{3}$$

where S is the area of the electrode, d is the thickness of the membrane, and R is the impedance.

2.9 Methanol permeability

Methanol permeability was tested using a diffusion cell consisting of two chambers (A and B) separated by a membrane. Chamber A is filled with a solution of 5.0 M methanol and 0.40 M H_2SO_4 in deionized H_2O. Chamber B is filled with distilled water. The methanol permeation through the membrane is due to the difference in concentration between chambers A and B. The methanol concentration in chamber B was measured every 15 min for 2 h by gas chromatography (GC). The methanol permeability can be calculated according to the following equation.

$$C_B(t) = \frac{A}{V_B} \frac{P}{L} C_A(t - t_0) \tag{4}$$

where P is the methanol permeability, $C_B(t)$ is the concentration of methanol in permeate (chamber B), C_A is the concentration of methanol in the feed (chamber A), A and L are the membrane area and thickness, and V_B is the volume of permeate in chamber B. The methanol permeability (P) in Eq. (4) is directly proportional to the slope of the linear expression for the concentration of methanol in chamber B as the Y ordinate versus time ($t - t_0$) as the X-axis.

$$P = \frac{dC_B(t)}{dt} \frac{V_B}{A} \frac{L}{C_A} \tag{5}$$

where $\frac{dC_B(t)}{dt}$ is the slope of the linear function of C_B versus t in Eq. (4).

2.10 Membrane electrode assembly (MEA) fabrication and fuel cell test

The catalyst ink was prepared from Pt/C catalyst (40 wt.% Pt, Johnson Mattey Corp.), 5 wt.% Nafion® solution, isopropyl alcohol, and de-ionized water. Water was added dropwise to moisturize the catalyst, and then 5 wt.%

Nafion® with isopropyl alcohol was added dropwise to form the ink. The mixture was dispersed by an ultrasonic stirrer bath for 20 min to form the catalyst slurry. The electrodes were prepared by directly spraying the catalyst slurry on 2 cm × 2 cm carbon papers (EC-TP1–060, Electrochem. Inc.) and subsequently drying at 60 °C under vacuum. The Pt loading was 0.4 mg/cm^2, and the mass ratio of dry Nafion® to Pt/C is 1:4. A membrane was sandwiched between two pieces of electrodes and then hot pressed.

The performance of the membrane-electrode assembly (MEA) was tested using a 4 cm^2 single cell in humidified H$_2$/O$_2$ (for PEMFC), and 1.0 M methanol/humidified O$_2$ (for direct methanol fuel cell (DMFC)), respectively. For PEMFC, the single cell was operated at 85 °C under 100% relative humidity (RH) with 0 MPa gas back-pressure. The gas feeding rate of oxygen was fixed at twice of hydrogen to provide adequate oxidant for the fuel. For DMFC, the single cell was operated at 80 °C at ambient pressure. The polarization curves were measured by applying a constant current for 1 min at each point using a fuel cell test station (Arbin Instruments, 160,269). The power densities were calculated from the steady-state voltages and applied currents.

3 Results and discussion

3.1 Compositional and morphological analysis

The representative FT-IR spectra of ZrP, ZrP-SH, ZrP-SO$_3$H, SPFEK, and SPFEK/ZrP-SO$_3$H composite membrane are shown in Fig. 2. In the spectra of ZrP and ZrP-SH, the samples exhibit a broad band peaked at ca. 1057 cm^{-1} due to the overlap of P-O and Zr-O peaks. There are two absorption
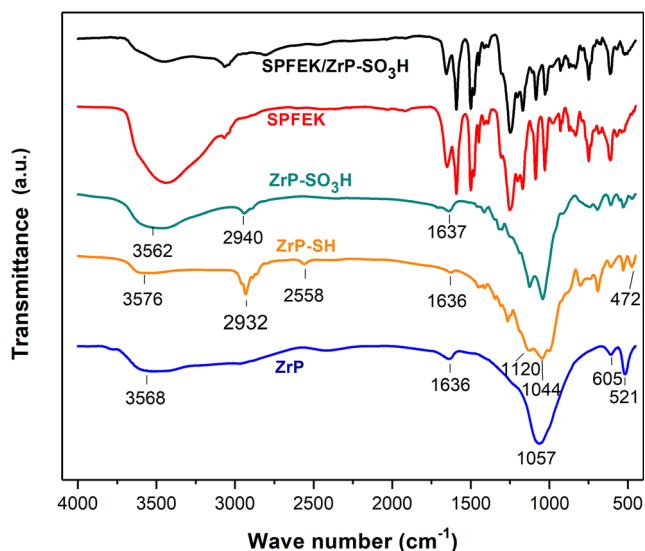

Fig. 2 FT-IR spectra of ZrP, ZrP-SH, ZrP-SO$_3$H, SPFEK, and SPFEK/ZrP-SO$_3$H composite membrane

bands at ~3570 and 1636 cm^{-1}, assigned to the stretching vibration and bending vibrations of –OH groups, respectively. The additional peaks at 472, 1120, 2558, and 2932 cm^{-1} in the spectrum of ZrP-SH are ascribed to the Si-O-Si bending vibration, Si-O-Si symmetric stretching vibration, S-H stretching vibration of thiol groups, and C-H stretching vibration of methylene groups, respectively, suggesting the successful graft reaction of MTPMS with ZrP. In the spectra of ZrP-SO$_3$H, the absence of a peak at 2558 cm^{-1} indicates that all thiol groups attached to the ZrP-SH have been oxidized to sulfonic acid groups, indicating the successful synthesis of ZrP-SO$_3$H. Furthermore, the bands ranging from 1000 to 1126 cm^{-1} are complicated due to the overlap of S-O symmetric and asymmetric stretching vibration of sulfonic acid groups (1084 and 1029 cm^{-1}) with Si-O-Si symmetric stretching vibration, as well as P-O stretching vibration.

In order to investigate the distribution of the functionalized ZrP nanosheets in the composite membranes, SEM-EDX was applied to the cross-section of the composite membranes, as depicted in Fig. 3. The ZrP-SO$_3$H fillers were well dispersed throughout the SPFEK-ZrP-2% composite membrane (Fig. 3a). When the filler loading was increased to 4%, aggregation of ZrP-SO$_3$H fillers within some regions were observed (Fig. 3b). Similarly, as shown in Fig. 3c and d, based on the cross-sectional images with linear analysis of Zr atom content along the transverse direction of the composite membranes by EDX, SPFEK/ZrP-SO$_3$H nanosheets were virtually uniformly dispersed in SPFEK/ZrP-SO$_3$H-2%, but a lower level of dispersion was achieved in SPFEK/ZrP-SO$_3$H-4%. Nevertheless, no aggregation was observed at the bottom of the membranes.

3.2 Water uptake and proton conductivity

The water within the membrane plays a vital role in the transportation of protons (vehicle mechanism or the Grotthuss mechanism) [53–55], which affects the overall FC performance significantly. The water uptake of the membranes is dependent on several parameters, including content and distribution of sulfonic acid groups, temperature, and relative humidity. Generally, the water uptake increases with the increase of membranes' IEC and temperature. Although a larger water uptake facilitates proton transportation to a greater extent, excessive water uptake could result in an apparent decrease in mechanical strength of the membrane and a dimensional mismatch between the membrane and the electrodes. The IEC value of ZrP-SO$_3$H was tested to be 2.81 meq/g, which is higher than the value of SPFEK (1.75 meq/g). As shown in Table 1, the IEC values of the SPFEK/ZrP-SO$_3$H composite membranes increased with an increasing doping degree. On the other hand, the water uptake of SPFEK barely changed after the incorporation of SPFEK/ZrP-SO$_3$H nanosheets. As is known, the water absorption of polymers usually depends on the concentration of sulfonic acid groups. In our

Fig. 3 SEM images of the cross-section of (**a**) SPFEK/ZrP-SO₃H-2% and (**b**) SPFEK/ZrP-SO₃H-4% composite membranes; SEM images with zirconium concentration profile of (**c**) SPFEK/ZrP-SO₃H-2% and (**d**) SPFEK/ZrP-SO₃H-4% composite membranes
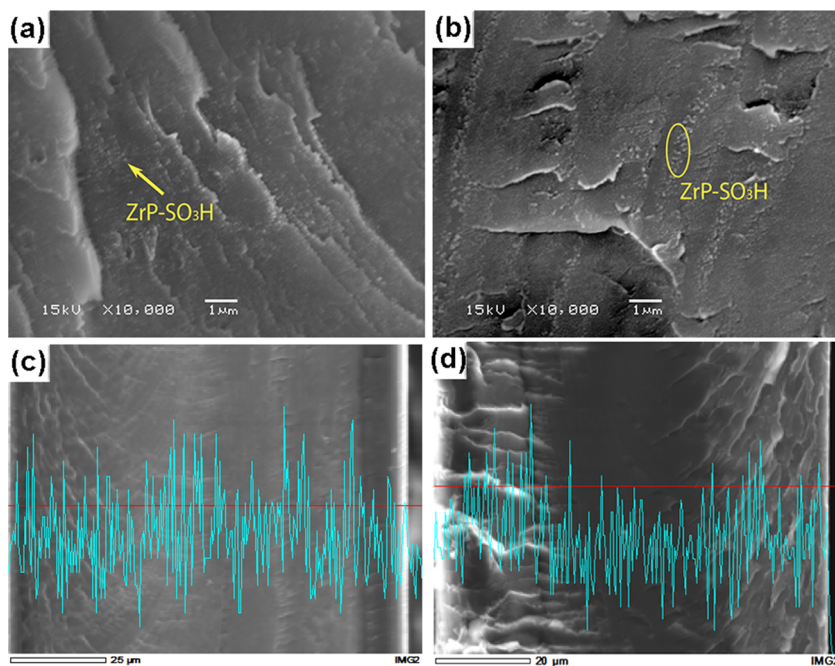
investigation, the water uptake of the composite membranes showed an almost constant value. These results suggest that the addition of ZrP-SO₃H nanosheets is effective in elevating IEC values of the resultant composite membranes without increasing water absorption. The introduction of ZrP-SO₃H nanosheets leads to a high concentration of sulfonic acid groups within the membrane, which should enhance water uptake. However, the ZrP-SO₃H nanosheets locate at the interspace of the macromolecular chains and occupy some space of water molecules. The combined effects balance the water uptake to a virtually constant value. A similar phenomenon was reported in the literature [56].

Proton conductivity was measured under the fully hydrated condition at 80 °C. Table 1 clearly reveals that the

incorporation of ZrP-SO₃H nanosheets into the SPFEK matrix can significantly improve its proton conductivity. These results can be ascribed to the increased concentration of sulfonic acid groups, which enhances the proton transfer.

3.3 Oxidative stability

Chemical stability of proton exchange membranes is one of the most important factors that affect their durability. It is well known that the formation of HO· and HOO· radicals from the catalytic process during FC operation causes membrane degradation [57]. Fenton's reagent is often used for the determination of a membrane's stability, for an accelerated testing. The highly reactive HO· and HOO· radicals generated by Fenton's reagent can attack the polymer main chains and result in considerable degradation of composite membranes. The oxidative stability of the SPFEK/ZrP-SO₃H composite membranes was examined by the weight loss and IEC loss of the membranes after being treated in Fenton's reagent for

Table 1 Water uptake and proton conductivity of pure SPFEK, SPFEK/ZrP-SO₃H-2% and SPFEK/ZrP-SO₃H-4% composite membranes, and Nafion® 117

Membrane	IEC^a (meq/g)	Water uptake^b (%) 80 °C	Proton conductivity^c (mS/cm) 80 °C
SPFEK	1.75	46.8	27.1
SPFEK/ZrP-SO₃H-2%	1.79	46.3	31.3
SPFEK/ZrP-SO₃H-4%	1.85	43.3	47.5
Nafion® 117	0.93	40.1	49.7

^{a} Calculated based on titration

^{b} Measured after equalized in deionized water for 24 h

^{c} Measured at 100% relative humidity

Table 2 Oxidative stability of pure SPFEK, SPFEK/ZrP-SO₃H-2% and SPFEK/ZrP-SO₃H-4% composite membranes, and Nafion® 117

Membrane	IEC loss (%)	Weight loss (%)
SPFEK	7.1	13.1
SPFEK/ZrP-SO₃H-2%	−4.7	5.3
SPFEK/ZrP-SO₃H-4%	−6.5	4.9
Nafion® 117	2.1	3.9

1 h. As shown in Table 2, both SPFEK/ZrP-SO₃H composite membranes show significantly enhanced oxidative stability than the neat SPFEK membrane. The weight losses of both composite membranes are much lower than that of the neat SPFEK membrane. In particular, SPFEK/ZrP-SO$_3$H-2% membrane demonstrates that a small amount of ZrP-SO$_3$H is effective in enhancing oxidative stability. It should be noted that, after the treatment by Fenton's reagent, the IEC value of the composite membrane increased with the ZrP-SO$_3$H content. This may be caused by the acidic hydroxyl groups in ZrP-SO$_3$H. Before the test of oxidative stability, due to the interactions between the –OH and –SO$_3$H groups of ZrP-SO$_3$H, the proton-donating ability of –OH is low and protons are more difficult to exchange via Na$^+$ during the titration. After the treatment by Fenton's reagent, the membrane became less dense, and the protons on the –OH groups in ZrP-SO$_3$H can be easily exchanged by Na$^+$ cations. Thus, the IEC of SPFEK/ ZrP-SO$_3$H composite membranes became higher. The phenomenon that IEC rose after an oxidative stability test was also reported by other researchers [56]. Meanwhile, the IEC loss and weight loss of Nafion® 117 are much lower than that of SPFEK, mainly because Nafion® 117 is a fluoropolymer, where fluorine atoms protect the polymer chains from being attacked by water molecules containing highly oxidizing radical species [57].

3.4 Thermal properties

Thermal properties of SPFEK/ZrP-SO$_3$H composite membranes in their acid form were characterized by TGA, and the results are shown in Fig. 4. The degradation of pure SPFEK has two major steps. The first weight loss is assigned to the elimination of sulfonic acid groups, which occurred during a temperature range of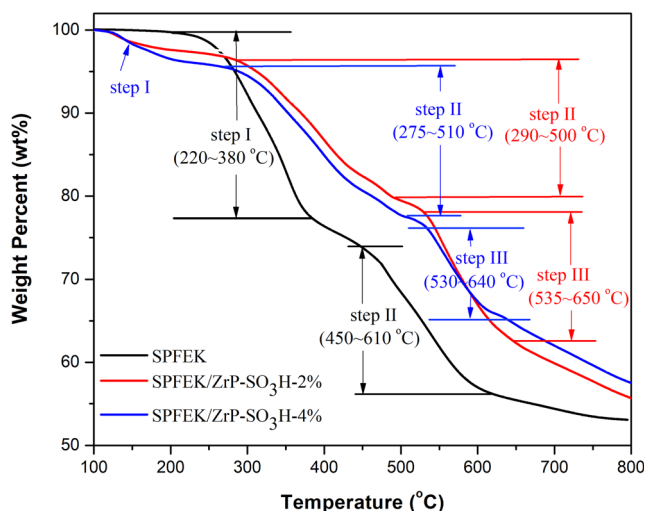 220–380 °C. The second weight loss at about 450–610 °C is due to the decomposition of the polymer main chains. The composite membranes exhibit a three-step degradation. The additional weight loss before 200 °C (step I) is corresponding to the removal of hydration water of ZrP-SO$_3$H [34, 58, 59]. Overall, the TGA thermograms of SPFEK/ZrP-SO$_3$H composite membranes are similar to that of the neat SPFEK membrane. Note that the decomposition temperature of the polymer main chains (step III in Fig. 4) rises to 530 °C for SPFEK/ZrP-SO$_3$H-2% and 535 °C for SPFEK/ZrP-SO$_3$H-4%, which are much higher than that of pure SPFEK (450 °C). The increase in decomposition temperature implies that the existence of thermally stable ZrP-SO$_3$H nanosheets can help improve the thermal stability of the resultant composite membranes without changing the decomposition mechanism. In addition, SPFEK/ZrP-SO$_3$H-2% with a lower ZrP-SO$_3$H weight content shows less weight loss of hydration water in the first step but more weight loss overall, compared with SPFEK/ZrP-SO$_3$H-4%. The hydration water in the membrane samples was mainly retained by ZrP-SO$_3$H; thus a lower weight content of ZrP-SO$_3$H corresponded to less hydration water loss. Meanwhile, ZrP-SO$_3$H nanosheets are more thermally stable than SPFEK, and their presence helped further improve the thermal stability of SPFEK. As a result, SPFEK/ZrP-SO$_3$H-4% exhibited less weight loss overall.

3.5 Single PEMFC performance

The polarization and power density curves of the H$_2$/O$_2$ fuel cells assembled with the composite membranes SPFEK/ZrP-SO$_3$H-2% and SPFEK/ZrP-SO$_3$H-4% are shown in Fig. 5a. Both SPFEK and Nafion® 117 were used as controls. All single PEMFCs were performed at a cell temperature of 85 °C, 100% relative humidity, with a back-gas pressure of 0 MPa. The open-circuit voltages (OCV) of the fuel cells composed of SPFEK/ZrP-SO$_3$H-2%, SPFEK/ZrP-SO$_3$H-4%, SPFEK, and Nafion® 117 were 0.99, 0,98, 0.98, and 0.99 V, respectively. This indicates that all membranes exhibit very close gas permeability. The highest current densities of the fuel cells using SPFEK/ZrP-SO$_3$H-2%, SPFEK/ZrP-SO$_3$H-4%, SPFEK, and Nafion® 117 were 1.29, 0.93, 1.09, and 1.15 A/cm^2, respectively, with a cut-off voltage of 0.1 V; the highest power densities of the four corresponding fuel cells were 0.268, 0.198, 0.255, and 0.271 W/cm^2, respectively. It is obvious that the fuel cell using composite membrane SPFEK/ZrP-SO$_3$H-2% exhibited better performance than the fuel cell using neat SPFEK. However, similar to many other composites [34, 35, 60], a higher filler loading does not guarantee better results. The fuel cell using SPFEK/ZrP-SO$_3$H-4% exhibited reduced performance. This is probably because excessive ZrP-SO$_3$H nanosheets resulted in a non-uniform distribution, which was observed from the SEM results. This could explain why SPFEK/ZrP-SO$_3$H-4% had a high proton conductivity but gave inferior fuel cell performance.
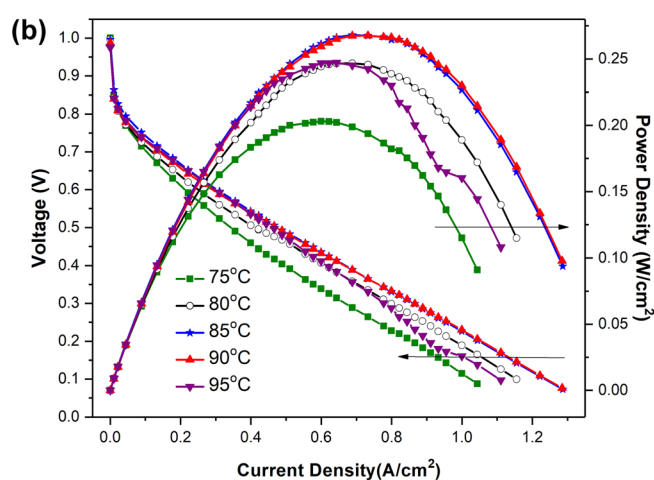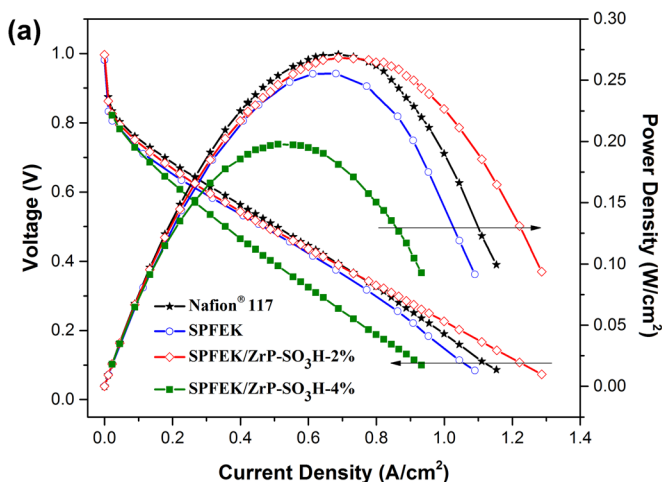

Fig. 4 TGA thermograms of pure SPFEK, SPFEK/ZrP-SO₃H-2%, and SPFEK/ZrP-SO₃H-4% composite membranes

Fig. 5 (**a**) Polarization and power density curves of the PEMFCs using SPFEK, Nafion® 117, SPFEK/ZrP-SO$_3$H-2%, and SPFEK/ZrP-SO$_3$H-4% as PEMs operating at 85 °C; (**b**) polarization and power density curves of a PEMFC using SPFEK/ZrP-SO$_3$H-2% at different temperatures

It was very encouraging that membrane SPFEK/ZrP-SO$_3$H-2% exhibited a comparable cell performance with Nafion® 117 in H$_2$/O$_2$ fuel cells. The polarization and power density curves of a H$_2$/O$_2$ fuel cell using SPFEK/ZrP-SO$_3$H-2% at temperatures of 75, 80, 85, 90 and 95 °C at 100% RH and ambient pressure were recorded and are shown in Fig. 5b. In the temperature range of 75 ~ 85 °C, the fuel cell performance significantly increased with the operating temperature. When the temperature reached 90 °C, the cell showed the highest current density of 1.29 A/cm^2 and a power density of 0.26 W/cm^2, which was the same as a fuel cell operated at 85 °C. However, when the temperature was further elevated to 95 °C, cell performance dropped. This is probably because at such a high temperature, the water retentivity of the membrane decreased, and hence the proton conductivity decreased. In brief, the fuel cell using composite membrane SPFEK/ZrP-SO$_3$H-2% displayed an optimal working temperature of 85 ~ 90 °C.

SPFEK/ZrP-SO$_3$H-2% composite membrane was further investigated in a DMFC. DMFCs using SPFEK/ZrP-SO$_3$H-2%, SPFEK, and Nafion® 117 as PEMs were tested at 80 °C with 1.0 M methanol and humidified oxygen gas at ambient pressure. As expected, the methanol permeability of the composite membranes decreased with an increasing ZrP-SO$_3$H content in the composite membrane (Table 3), indicating the composite membranes have better methanol resistances. The methanol

permeability of SPFEK/ZrP-SO$_3$H-2% is 2.25×10^{-7} cm^2 s^{-1}, which is only ca. 15.4% of the value of Nafion® 117 (1.46×10^{-6} cm^2 s^{-1}). These results are consistent with another report of a composite membrane using SiO$_2$ as fillers [61]. As shown in Fig. 6, there is a marked improvement in DMFC performance for the cell composed of SPFEK/ZrP-SO$_3$H-2%. The DMFC using SPFEK/ZrP-SO$_3$H-2% shows a peak power density of 61 mW/cm^2, which is much higher than 38 and 41 mW/cm^2 for the DMFCs using SPFEK and Nafion® 117, respectively. Because the methanol permeability and membrane conductivity serve as two key parameters in DMFC performances, the composite membrane SPFEK/ZrP-SO$_3$H-2% possessing low methanol permeability and high membrane conductivity exhibited the best DMFC performance. Overall, the composite membrane with conductive ZrP-SO$_3$H nanosheets displayed significant improvement in DMFC performance. These results

Table 3 Methanol permeability (cm^2 s^{-1}) of Nafion® 117, pure SPFEK, SPFEK/ZrP-SO$_3$H-2% and SPFEK/ZrP-SO$_3$H-4% composite membranes at 80 °C

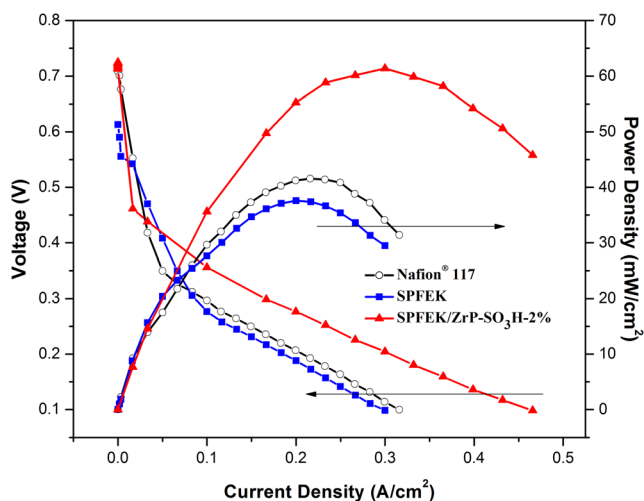| Nafion® 117	SPFEK	SPFEK-ZrP-SO$_3$H-2%	SPFEK-ZrP-SO$_3$H-4%
1.46×10^{-6}	3.06×10^{-7}	2.25×10^{-7}	1.36×10^{-7}

Fig. 6 Polarization and power density curves of DMFCs using SPFEK/ZrP-SO$_3$H-2%, SPFEK, and Nafion® 117 as PEMs, using 1.0 M methanol at 80 °C

demonstrate that the ZrP-SO₃H-doped SPFEK membrane is a promising candidate for polymer electrolyte membranes for high-performance DMFCs.

4 Conclusion

A functionalized proton conductive filler ZrP-SO₃H was synthesized and used to prepare SPFEK/ZrP-SO₃H composite membranes with 2 wt.% and 4 wt.% filler loadings. When the loading was 2 wt.%, a uniform dispersion of ZrP-SO₃H nanosheets was achieved in the composite membrane SPFEK/ZrP-SO₃H-2%. The composite membranes showed improved proton conductivity, oxidative stability, and methanol barrier property. SPFEK/ZrP-SO₃H-2% exhibited better fuel cell performance than neat SPFEK in the H_2/O_2 fuel cell test. Moreover, in the DMFC test, SPFEK/ZrP-SO₃H-2% showed a peak power density of 61 mW/cm², which is much higher than 38 and 41 mW/cm² for the DMFCs using SPFEK and Nafion® 117, respectively. These results show that the incorporation of ZrP-SO₃H to SPFEK is effective in improving fuel cell performances in all respects. The SPFEK/ZrP-SO₃H-2% membrane is promising for high-performance H_2/O_2 fuel cells and DMFCs as a polymer electrolyte membrane.

Compliance with ethical standards

Competing interests The authors declare that they have no known competing financial interests or personal relationships that could have appeared to influence the work reported in this paper.

References

1. Steele BCH, Heinzel A (2001) Materials for fuel-cell technologies. Nature 414:345–352

2. Veziroglu A, Macario R (2011) Fuel cell vehicles: state of the art with economic and environmental concerns. Int J Hydrogen Energy 36:25–43

3. Roziere J, Jones DJ (2003) Non-fluorinated polymer materials for proton exchange membrane fuel cells. Annu Rev Mater Res 33:503–555

4. Mauritz KA, Moore RB (2004) State of understanding of Nafion. Chem Rev 104:4535–4585

5. Hickner MA, Ghassemi H, Kim YS, Einsla BR, McGrath JE (2004) Alternative polymer systems for proton exchange membranes (PEMs). Chem Rev 104:4587–4612

6. McGrath JE, Hickner MA, Ghassemi H, Kim YS, Einsla BR (2004) Alternative polymer systems for proton exchange membranes (PEMs). Chem Rev 104:4587–4611

7. Kuzmenko M, Poryadchenko N (2005) Perspective materials for application in fuel-cell technologies. In: Sammes N (ed) Fuel cell technologies: state and perspectives. Springer, Netherlands, pp 253–258

8. Zhai L, Li H (2019) Polyoxometalate-polymer hybrid materials as proton exchange membranes for fuel cell applications. Molecules 24:3425

9. Han X, Xie Y, Liu D, Chen Z, Zhang H, Pang J, Jiang Z (2019) Synthesis and properties of novel poly(arylene ether)s with densely sulfonated units based on carbazole derivative. J Membr Sci 589:117230

10. Kwon S, Kim T-H (2017) The effect of adjusting the hydrophilic-hydrophobic block length in densely sulfonated poly(fluorenyl ether sulfone) block copolymer membranes. Int J Hydrogen Energy 42:11845–11856

11. McGrath JE, Wang F, Hickner M, Kim YS, Zawodzinski TA (2002) Direct polymerization of sulfonated poly(arylene ether sulfone) random (statistical) copolymers: candidates for new proton exchange membranes. J Membr Sci 197:231–242

12. Schuster M, Kreuer KD, Andersen HT, Maier J (2007) Sulfonated poly(phenylene sulfone) polymers as hydrolytically and thermooxidatively stable proton conducting ionomers. Macromolecules 40:598–607

13. Watanabe M, Yasuda T, Li Y, Miyatake K, Hirai M, Nanasawa M (2006) Synthesis and properties of polyimides bearing acid groups on long pendant aliphatic chains. J Polym Sci A Polym Chem 44:3995–4005

14. Meng Y, Wang L, Wang S, Shang X, Li L, Hay AS (2004) Synthesis and sulfonation of poly(aryl ethers) containing triphenyl methane and tetraphenyl methane moieties from isocynate-masked bisphenols. Macromolecules 37:3151–3158

15. Kreuer KD (2001) On the development of proton conducting polymer membranes for hydrogen and methanol fuel cells. J Membr Sci 185:29–39

16. Chen Y, Meng Y, Wang S, Tian S, Chen Y, Hay AS (2006) Sulfonated poly(fluorenyl ether ketone) membrane prepared via direct polymerization for PEM fuel cell application. J Membr Sci 280:433–441

17. Zarrin H, Higgins D, Jun Y, Chen Z, Fowler M (2011) Functionalized graphene oxide nanocomposite membrane for low humidity and high temperature proton exchange membrane fuel cells. J Phys Chem C 115:20774–20781

18. Tripathi BP, Shahi VK (2008) Functionalized organic-inorganic nanostructured N-p-carboxy benzyl chitosan-silica-PVA hybrid polyelectrolyte complex as proton exchange membrane for DMFC applications. J Phys Chem B 112:15678–15690

19. Holdcroft S, Thomas OD, Peckham TJ, Thanganathan U, Yang YS (2010) Sulfonated polybenzimidazoles: proton conduction and acid-base crosslinking. J Polym Sci A Polym Chem 48:3640–3650

20. Manthiram A, Zhao JA, Jarvis K, Ferreira P (2011) Performance and stability of Pd-Pt-Ni nanoalloy electrocatalysts in proton exchange membrane fuel cells. J Power Sources 196:4515–4523

21. Yilmazturk S, Deligoz H, Yilmazoglu M, Damyan H, Oksuzomer F, Koc SN, Durmus A, Gurkaynak MA (2009) A novel approach for highly proton conductive electrolyte membranes with improved methanol barrier properties: layer-by-layer assembly of salt containing polyelectrolytes. J Membr Sci 343:137–146

22. Jiang SP, Liu ZC, Tian ZQ (2006) Layer-by-layer self-assembly of composite polyelectrolyte-nafion membranes for direct methanol fuel cells. Adv Mater 18:1068–1072

23. Wang S, Zhang G, Han MM, Li HT, Zhang Y, Ni J, Ma WJ, Li MY, Wang J, Liu ZG, Zhang LY, Na H (2011) Novel epoxy-based cross-linked polybenzimidazole for high temperature proton exchange membrane fuel cells. Int J Hydrogen Energy 36:8412–8421

24. Lee YM, Phu DS, Lee CH, Park CH, Lee SY (2009) Synthesis of Crosslinked sulfonated poly(phenylene sulfide sulfone nitrile) for direct methanol fuel cell applications. Macromol Rapid Commun 30:64–68

25. Sakamoto M, Nohara S, Miyatake K, Uchida M, Watanabe M, Uchida H (2015) Effects of SiO_2 nanoparticles incorporated into poly(arylene ether sulfone ketone) multiblock copolymer electrolyte membranes on fuel cell performance at low humidity. Electrochemistry 83:150–154

26. Nawn G, Pace G, Lavina S, Vezzu K, Negro E, Bertasi F, Polizzi S, Di Noto V (2015) Nanocomposite membranes based on polybenzimidazole and ZrO_2 for high-temperature proton exchange membrane fuel cells. Chemsuschem 8:1381–1393

27. Park KT, Jung UH, Choi DW, Chun K, Lee HM, Kim SH (2008) ZrO_2–SiO_2/Nafion® composite membrane for polymer electrolyte membrane fuel cells operation at high temperature and low humidity. J Power Sources 177:247–253

28. Choi YS, Kim TK, Kim EA, Joo SH, Pak C, Lee YH, Chang H, Seung D (2008) Exfoliated Sulfonated poly(arylene ether sulfone)–clay Nanocomposites. Adv Mater 20:2341–2344

29. Liu KL, Lee HC, Wang BY, Lue SJ, Lu CY, Tsai LD, Fang J, Chao CY (2015) Sulfonated poly(styrene-block-(ethylene-ran-butylene)-block-styrene (SSEBS)-zirconium phosphate) (ZrP) composite membranes for direct methanol fuel cells. J Membr Sci 495:110–120

30. Pandey J, Seepana MM, Shukla A (2015) Zirconium phosphate based proton conducting membrane for DMFC application. Int J Hydrogen Energy 40:9410–9421

31. Sahu AK, Ketpang K, Sharmaugam S, Kwon O, Lee S, Kim H (2016) Sulfonated graphene-nafion composite membranes for polymer electrolyte fuel cells operating under reduced relative humidity. J Phys Chem C 120:15855–15866

32. Sahu AK, Pitchumani S, Sridhar P, Shukla AK (2009) Co-assembly of a nafion-mesoporous zirconium phosphate composite membrane for PEM fuel cells. Fuel Cells 9:139–147

33. Sigwadi R, Dhlamini MS, Mokrani T, Nemavhola F, Nonjola PF, Msomi PF (2019) The proton conductivity and mechanical properties of Nafion®/ ZrP nanocomposite membrane. Heliyon 5:e02240

34. Mazzapioda L, Panero S, Navarra MA (2019) Polymer electrolyte membranes based on nafion and a superacidic inorganic additive for fuel cell applications. Polymers 11:914

35. Yao Y, Lin Z, Li Y, Alcoutlabi M, Hamouda H, Zhang X (2011) Superacidic electrospun fiber-nafion hybrid proton exchange membranes. Adv Energy Mater 1:1133–1140

36. Boo WJ, Sun L, Liu J, Clearfield A, Sue H-J (2007) Effective intercalation and exfoliation of nanoplatelets in epoxy via creation of porous pathways. J Phys Chem C 111:10377–10381

37. Sun L, Boo WJ, Sue H-J, Clearfield A (2007) Preparation of alpha-zirconium phosphate nanoplatelets with wide variations in aspect ratios. New J Chem 31:39–43

38. Hu H, Martin JC, Xiao M, Southworth CS, Meng Y, Sun L (2011) Immobilization of ionic liquids in layered compounds via mechanochemical intercalation. J Phys Chem C 115:5509–5514

39. Hu H, Martin JC, Zhang M, Southworth CS, Xiao M, Meng Y, Sun L (2012) Immobilization of ionic liquids in theta-zirconium phosphate for catalyzing the coupling of CO_2 and epoxides. RSC Adv 2:3810–3815

40. Wang Q, Yu J, Liu J, Guo Z, Umar A, Sun L (2013) Na^+ and K^+-exchanged zirconium phosphate (ZrP) as high-temperature CO_2 adsorbents. Sci Adv Mater 5:469–474

41. Lu N, Lin K-Y, Kung C-C, Jhuo J-W, Zhou Y, Liu J, Sun L (2014) Intercalated polyfluorinated Pd complexes in alpha-zirconium phosphate for Sonogashira and heck reactions. RSC Adv 4:27329–27336

42. Boo WJ, Sun L, Warren GL, Moghbelli E, Pham H, Clearfield A, Sue HJ (2007) Effect of nanoplatelet aspect ratio on mechanical properties of epoxy nanocomposites. Polymer 48:1075–1082

43. Sun L, Boo WJ, Sun D, Clearfield A, Sue H-J (2007) Preparation of exfoliated epoxy/alpha-zirconium phosphate nanocomposites containing high aspect ratio nanoplatelets. Chem Mater 19:1749–1754

44. Sun L, O'Reilly JY, Kong D, Su JY, Boo WJ, Sue HJ, Clearfield A (2009) The effect of guest molecular architecture and host crystallinity upon the mechanism of the intercalation reaction. J Colloid Interface Sci 333:503–509

45. Zhou Y, Wang A, Wang Z, Chen M, Wang W, Sun L, Liu X (2015) Titanium functionalized alpha-zirconium phosphate single layer nanosheets for photocatalyst applications. RSC Adv 5:93969–93978

46. Zhou Y, Liu J, Xiao M, Meng Y, Sun L (2016) Designing supported ionic liquids (ils) within inorganic nanosheets for CO_2 capture applications. ACS Appl Mater Interfaces 8:5547–5555

47. Laipan M, Xiang L, Yu J, Martin BR, Zhu R, Zhu J, He H, Clearfield A, Sun L (2020) Layered intercalation compounds: mechanisms, new methodologies, and advanced applications. Prog Mater Sci 109:100631

48. Boo WJ, Sun LY, Liu J, Clearfield A, Sue HJ, Mullins MJ, Pham H (2007) Morphology and mechanical behavior of exfoliated epoxy/alpha-zirconium phosphate nanocomposites. Compos Sci Technol 67:262–269

49. Zhou Y, Huang R, Ding F, Brittain AD, Liu J, Zhang M, Xiao M, Meng Y, Sun L (2014) Sulfonic acid-functionalized alpha-zirconium phosphate single-layer nanosheets as a strong solid acid for heterogeneous catalysis applications. ACS Appl Mater Interfaces 6:7417–7425

50. Zhou Y, Noshadi I, Ding H, Liu J, Parnas RS, Clearfield A, Xiao M, Meng Y, Sun L (2018) Solid acid catalyst based on single-layer alpha-zirconium phosphate nanosheets for biodiesel production via esterification. Catalysts 8:17

51. Wang F, Chen TL, Xu JP (1998) Sodium sulfonate-functionalized poly(ether ether ketone)s. Macromol Chem Phys 199:1421–1426

52. Shang X, Tian S, Kong L, Meng Y (2005) Synthesis and characterization of sulfonated fluorene-containing poly(arylene ether ketone) for proton exchange membrane. J Membr Sci 266:94–101

53. Peckham TJ, Holdcroft S (2010) Structure-morphology-property relationships of non-perfluorinated proton-conducting membranes. Adv Mater 22:4667–4690

54. Li N, Guiver MD (2014) Ion transport by nanochannels in ion-containing aromatic copolymers. Macromolecules 47:2175–2198

55. Shin DW, Guiver MD, Lee YM (2017) Hydrocarbon-based polymer electrolyte membranes: importance of morphology on ion transport and membrane stability. Chem Rev 117:4759–4805

56. Pan J, Wang S, Xiao M, Hickner M, Meng Y (2013) Layered zirconium phosphate sulfophenylphosphonates reinforced sulfonated poly (fluorenyl ether ketone) hybrid membranes with high proton conductivity and low vanadium ion permeability. J Membr Sci 443:19–27

57. Hu H, Xiao M, Wang SJ, Shen PK, Meng YZ (2011) Surface fluorination of poly(fluorenyl ether ketone) ionomers as proton exchange membranes for fuel cell application. Fuel Cells 11:353–360

58. Clearfield A, Costantino U (1996) Layered metal phosphates and their intercalation chemistry. In: Alberti G, Bein T (eds) Comprehensive supramolecular chemistry. Elsevier, Oxford, UK, pp 107–149

59. Zhou Y, Liu J, Huang R, Zhang M, Xiao M, Meng Y, Sun L (2017) Covalently immobilized ionic liquids on single layer nanosheets for heterogeneous catalysis applications. Dalton Trans 46:13126–13134

60. Ou Y, Tsen W-C, Jang S-C, Chuang F-S, Wang J, Liu H, Wen S, Gong C (2018) Novel composite polymer electrolyte membrane using solid superacidic sulfated zirconia - functionalized carbon nanotube modified chitosan. Electrochim Acta 264:251–259

61. Gonggo ST, Bundjali B, Hariyawati K, Arcana IM (2018) The influence of nano-silica on properties of sulfonated polystyrene-lignosulfonate membranes as proton exchange membranes for direct methanol fuel cell application. Adv Polym Technol 37:1859–1867